Journal of GeoEngineering, Vol. 14, No. 3, pp. 167-178, September 2019
http://dx.doi.org/10.6310/jog.201909_14(3).5

APPLICATION OF SYSTEM IDENTIFICATION FOR DYNAMIC CHARACTERISTICS OF ROCKING FOUNDATIONS

Yu-Wei Hwang [1], Jiunn-Shyang Chiou [2*], and Louis Ge [3]

ABSTRACT

This study applies system identification methods to analyze the change in the dynamic characteristics (fundamental frequency and damping ratio) of rocking foundation systems under earthquake excitation. Shaking table testing performed at the National Center for Research on Earthquake Engineering of Taiwan on a rocking-governed column-footing model is used for demonstration. Two methods of system identification, including short-time transfer function and autoregressive moving average (ARMA) model, are utilized to analyze the measured horizontal acceleration data. The segmental ARMA model is found effective to trace the change in the system fundamental frequency and damping ratio as well as the rotational stiffness of the footing. The system identification results show that during the shaking, the fundamental frequency (rotational stiffness of footing) and damping ratio of the system are not constant. As the shaking intensity increases, the fundamental frequency decreases along with the increasing damping ratio; however, the fundamental frequency goes up again and the damping ratio decreases as the shaking intensity decreases. Besides, the identified dynamic properties of the footing are consistent with those determined from the experimental moment-rotation curves of the footing.

Key words: Damping ratio, footings, fundamental frequency, rocking foundations, shaking table tests, system identification.

1. INTRODUCTION

In conventional structural analysis, the base of columns in a structural model is commonly assumed to be fixed (AASHTO 2009). For a structure with footings, the foundation is susceptible to rocking under strong seismic loading. The assumption of the fixed-base condition no longer holds and it may also produce different responses from actual ones. Besides, the seismic response of structure may be governed by the moment strength of the footings so that the expected hinging mechanism in the structure may not occur.

Many studies have been conducted to investigate the influence of foundation rocking on the response of structures under seismic loading (e.g., Gajan *et al.* 2005; Shirato *et al.* 2008; Paolucci *et al.* 2008; Gajan and Kutter 2008; Gazetas *et al.* 2013; Anastasopoulos and Kontoroupi 2014). From these studies, one of the major characteristics of rocking foundations is the uplift behavior of the footing, which leads to a reduction in the contact area between the soil and footing. Therefore, the rotational behavior of the footing can exhibit a nonlinear response even though the soil behaves less nonlinearly in stiff strata, and the dynamic characteristics of rocking foundation systems, including the fundamental frequency and equivalent damping ratio, may change during the excitation.

Manuscript received October 6, 2018; revised February 15, 2019; accepted March 23, 2019.

[1] Former graduate student, Department of Civil Engineering, National Taiwan University, Taipei, Taiwan 10617, R.O.C.

[2*] Assistant Professor (corresponding author), Department of Civil Engineering, National Taiwan University, Taipei, Taiwan 10617, R.O.C. (e-mail: jschiou@ntu.edu.tw).

[3] Professor, Department of Civil Engineering, National Taiwan University, Taipei, Taiwan 10617, R.O.C.

System identification is often used in the fields of automatic control and mechanical engineering. In geotechnical engineering, system identification has been applied to evaluate the dynamic behavior of soil layers under earthquakes (*e.g.,* Safak 1989; Zeghal *et al.* 1995; Elgamal *et al.* 1996; Mikami *et al.* 2003). When the input and output of a system are given, system identification can help determine the system parameters of interest such as the stiffness, damping ratio, and natural frequency. Polhemus and Cakmak (1981) used a time invariant autoregressive moving average (ARMA) model to determine the system parameters of a soil layer subjected to seismic loading by simulating the transfer function of ground acceleration responses. Glaser (1995) found that frequency based transfer functions may be inappropriate to nonstationary field data because finite time period and noise would cause aliasing and leakage on signals. For nonstationary data (time-varying systems), Glaser and Baie (2000) suggested utilizing a segmentation scheme to evaluate the changes in the system parameters with time by using a recursive parametric model, like the ARMA model.

This study makes an attempt to apply system identification approaches for the evolution of dynamic characteristics of a rocking footing. Shaking table tests conducted by Chiou *et al.* (2018) on a rocking-governed column-footing model is used for demonstration. Two identification methods, the transfer function (TF) and the autoregressive moving average model (ARMA), are adopted and their results are compared to evaluate their applicability. These two methods are for linearly time-invariant (LTI) systems. By dividing the entire time history into several segments, the methods are extended to time-varying systems for tracing the changes in system parameters with time, including the fundamental frequency and damping ratio of the system and the rotational stiffness of the footing. The analysis results are further interpreted by comparing them with those from the experimental hysteretic moment-rotation loops of the footing.

2. SYSTEM IDENTIFICATION

2.1 Short-Time Transfer Function

The short-time Fourier transform (STFT) is a modified Fourier transform used to determine the distributions of frequency and the corresponding phase angle for a selected time section in a signal. Generally, the algorithm of the STFT is to divide the whole signal into many shorter time windows in equal length and perform the Fourier transform on each time section separately. By this way, the Fourier amplitude-frequency-time relationships can be built. In practice, the STFT is performed through the convolution of the time window and the Fourier transform of the signal over time. This can be expressed in a two-dimensional form as:

$$A(t,f)=\int_{-\infty}^{\infty} w(t-\tau)\, a(\tau)\, e^{-i2\pi f\tau} d\tau \tag{1}$$

where $a(\tau)$ is the signal and $w(t-\tau)$ is the window function. Based on the Heisenberg uncertainty principle, since the resolution of the time domain and frequency domain is fixed, higher frequency resolution will lead to lower time resolution and vice versa. That is to say, a larger window gives better frequency resolution but worse time resolution, and a narrow window gives good time resolution but poor frequency resolution. The number of samples on which the window sections overlap will also affect the resolution: a smaller overlap between two neighboring windows may result in larger leakage of a signal.

The transfer function is a complex function over frequency domain to describe the relationship between the output and input signals. The transfer function $G(f)$ is defined as

$$G(f)=\frac{Y(f)}{X(f)} \tag{2}$$

where f is the frequency; $X(f)$ and $Y(f)$ are the Fourier spectra of input and output time histories, $x(t)$ and $y(t)$, respectively.

With the aid of transform function, the fundamental frequency of a system can be identified based on the frequency corresponding to the peak value of the transfer function.

Similar to STFT, the short-time transfer function method is to build the transfer functions of selected time sections in a signal. In this method, STFT is applied to acceleration records of input and output signals to compute the Fourier's amplitude ratios of output/ input motions (amplification factors) of each time window. By this way, the amplification factor-frequency-time relationships and the evolution of the fundamental frequency can be built. To have a better balance between the time and frequency resolution, an appropriate window size of 256 data points and a 50% length overlap of two neighboring windows were set.

2.2 ARMA Model (Autoregressive Moving Average Model)

In an ARMA model, considering a linear time invariant single input and single output (SISO) system, the dynamic response of the system can be expressed in a linear difference equation as follows (Safak 1989; Glaser and Baise 2000),

$$\begin{aligned} &y(t)+a_1 y(t-1)+a_2\, y(t-2)+\ldots+a_{n_a} y(t-n_a) \\ &\quad = b_0\, x(t)+b_1 x(t-1)+b_2\, x(t-2)+\ldots+b_{n_b} x(t-n_b) \end{aligned} \tag{3}$$

where $y(t)$ and $x(t)$ are the system output and input sequences at time t, respectively; a_i and b_i (i = 1, 2, ⋯, n) are the coefficients of the output and input sequences; the amount of n_a and n_b represent that the amounts of output/ input time points in the past required to describe the output at time t.

Through the z-transform, Eq. (3) can further be expressed as

$$\begin{aligned} &Y(z)+a_1 z^{-1}Y(z)+a_2 z^{-2}Y(z)+\cdots+a_{n_a} z^{-n_a}Y(z) \\ &\quad = b_0\, X(z)+b_1 z^{-1}X(z)+b_2 z^{-2}X(z-2)+\cdots \\ &\qquad +b_{n_b} z^{-n_b} X(z-n_b) \end{aligned} \tag{4}$$

Then, the equation can be rearranged to give the ratio of output and input signals, which is called the system transfer function as follows,

$$G(z)=\frac{Y(z)}{X(z)}=\frac{(b_0+b_1 z^{-1}+b_2 z^{-2}+\ldots+b_{n_b} z^{-n_b})}{(1+a_1 z^{-1}+a_2 z^{-2}+\ldots+a_{n_a} z^{-n_a})} \tag{5}$$

The roots of the polynomial of the output $Y(z)$ are the zeros of the transfer functions; the roots of the polynomial of the input $X(z)$ are the poles of the transfer function.

The transfer function can be rewritten in terms of the poles and zeros of $G(z)$ as:

$$G(z)=\frac{b_0(z-z_1)(z-z_2)\cdots(z-z_{n_b})}{(z-p_1)(z-p_2)\cdots(z-p_{n_a})} \tag{6}$$

where p_j (j = 1, 2, … n_a) are the poles of $G(z)$, and z_i (i = 1, 2, ⋯, n_b) are the zeros of $G(z)$.

The order of the polynomial of the input n_a determines the number of the vibration modes of the system. Since the roots of the polynomial are complex-conjugate, n_a is even and the number of the vibration modes of the system is half of n_a. Based on the poles p_j', the damping ratio ζ_j and the natural frequency f_j of each vibration mode j of the system are determined as (Safak 1989).

$$\xi_j=-\frac{\ln(r_j)}{\sqrt{\ln(r_j)^2+\phi_j^2}} \tag{7}$$

$$f_j=\frac{1}{2\pi\Delta t}\sqrt{\ln(r_j)^2+\phi_j^2} \tag{8}$$

where r_j and ϕ_j are the amplitude and the phase angle of the jth pole (p_j) of the system, and Δt represents the sampling time interval.

However, it should be noted that although more model parameters can improve the accuracy of the prediction, the identified frequency and damping ratio may be abnormal due to high order polynomial fitting. In other words, if too many model parameters are applied to describe the system, the model will fit the local fluctuation of test data (*i.e.,* overshooting effect), which may result in irrational results.

To apply the ARMA model to rocking foundation systems, based on the segmentation scheme, the original signal is divided into several time segments in equal length. Each signal segment is regarded as an independent linear time invariant system. As a result, the ARMA model is performed on each time interval to distinguish the changes in the dynamic characteristics of the column-

footing model. Since this approach assumes a linear response in each time segment, there is no need to use too many modal frequencies in each section. To avoid overfitting, we use fewer model parameters and do not use fixed values of n_a and n_b for each time segment. An iteration process is performed for each time segment to determine the associated suitable n_a and n_b. In general, the fitting percentage above 90% is appropriate to obtain better n_a and n_b without overfitting.

3. OVERVIEW OF SHAKING TABLE TESTING ON A COLUMN-FOOTING MODEL

In the shaking table testing conducted by Chiou *et al.* (2018), a rocking-governed column-footing model, as shown in Fig. 1, consisting of a column of height 80 cm and a footing of 40 cm × 40 cm, was designed. The slender ratio of the model (height of the model to width of footing) was nearly 2.64. This model is rocking dominated as its slender ratio is larger than one (Gajan and Kutter 2009).

The footing was designed as a surface footing to clarify the rocking behavior without the influence of footing embedment. The column was an open pipe pile, made of aluminum, with an outer diameter of 89 mm and a thickness of 3 mm. The weight of the model was 0.165 kN. Mass blocks with weights of 0.905 kN were placed on the top of the column to simulate the weight of a structure. The total weight of the model was 1.07 kN. The fixed-base fundamental period of the model was approximately 0.125 sec (frequency of 8 Hz). The column-footing model was put on a soil specimen of size 188 cm × 188 cm × 120 cm in a laminar box. The laminar shear box is composed of 15 layers of sliding frames to simulate the one dimensional ground response under horizontal seismic excitations.

The Vietnam sand specimen of a relative density of about 75% (dense sand) was prepared to represent a sturdy ground through compaction by layers. The mass density of the specimen was 1.585 t/m^3. Based on the plate loading tests, the static factor of safety for the weight of the model against vertical bearing capacity was larger than 23 (Chiou *et al.* 2018). The angle of internal friction of the soil was about 39°. According to the results of transfer function of a uniform soil layer later discussed, the equivalent shear wave velocity of the soil was 96 m/s and the corresponding maximum shear modulus were 14.6 MPa.

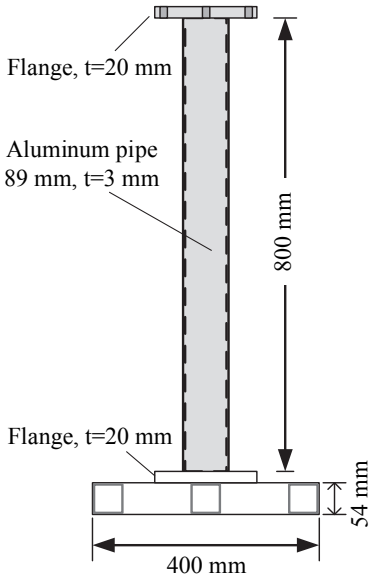

Fig. 1 The column-footing model (Chiou *et al.* 2018)

The sensors used in the testing included accelerometers, linear displacement transducers (LDT), and strain gauges. The accelerometers were used to measure the vertical and horizontal accelerations of the structure model and soil. The LVDTs were used to measure the horizontal displacement of the frames of the laminar box, which represented the lateral movements of the soil. In addition, many pictures were taken by an image measurement system to determine the movement of the structure model during the testing.

One-way excitation was applied at the bottom of the laminar box through the shaking table to simulate seismic loading. Three types of input motions were adopted, including white noise waves, sinusoid signals, and historical earthquake records (Chiou *et al.* 2018). Details for the test results can be found in Chiou *et al.* (2018).

4. ANALYSIS CASES

Four cases, as listed in Table 1, are adopted for analyses in this study. Cases 921-RSF-1 to 921-RSF-3 are the test cases subjected to a base motion using the record of TAP086 in Chi-Chi 921 Taiwan earthquake. The acceleration spectra of the earthquake events are shown in Fig. 2. Cases WN is the test case using a base motion of white noise signals conducted before Cases 921-RSF-1 to 921-RSF-3 for examining the initial characteristics of the footing-structure system.

Figure 3 shows the acceleration responses at the soil surface (in the direction of excitation), at the top of the footing (parallel with and normal to the direction of excitation), and at the top of the structure (in the direction of excitation) for Case 921-RSF-3. It can be seen that the acceleration at the top of the footing normal to the excitation direction is very small compared to the that parallel with the excitation direction, implying the yawing mode is slight; the acceleration at the top of the footing is close to the acceleration at the soil surface, indicating the translation mode is slight. However, the acceleration at the top of the structure is quite different from that at the soil surface due to the rocking mode. Figure 4 further compares the rotation histories at the top of the structure and at the top of the footing. It is found that the rotation histories are close, showing that the difference in acceleration responses at the top of the structure and the soil surface is mainly influenced by the rotational response of the footing (rocking mode). Therefore, in this study, the column-footing model is simplified as a single-degree-of-freedom rocking system, as shown in Fig. 5, which consists of a rigid bar with a mass on the top and a rotational spring at the base. The horizontal acceleration record at the surface of the soil is considered as the input motion, and the acceleration record at top of the mass is regarded as the output motion for system identification.

Table 1 Selected test cases for analysis

Case	Input motion	Max. acceleration (g)
WN	White noise bandwidth 60 Hz	0.03
921-RSF-1	Chichi earthquake (TAP086)	0.05
921-RSF-2	Chichi earthquake (TAP086)	0.20
921-RSF-3	Chichi earthquake (TAP086)	0.35

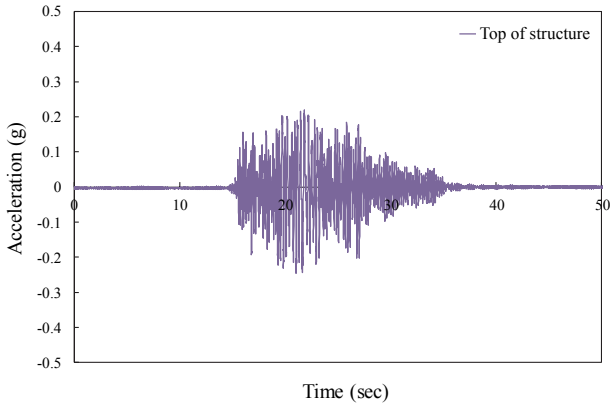

(a) Top of structure

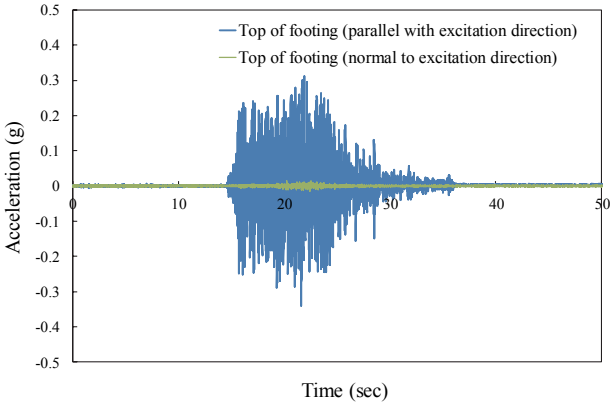

(b) Top of footing

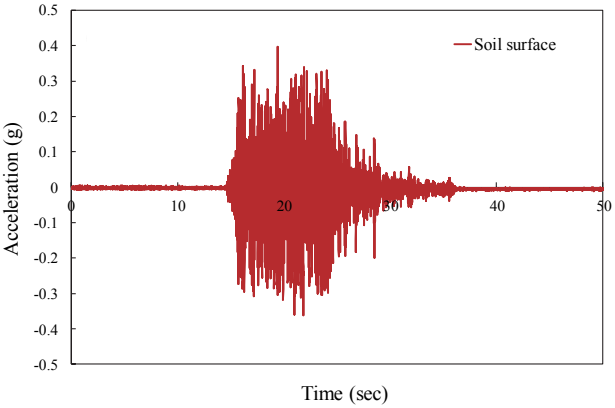

(c) Soil surface

Fig. 2 Comparison of acceleration histories

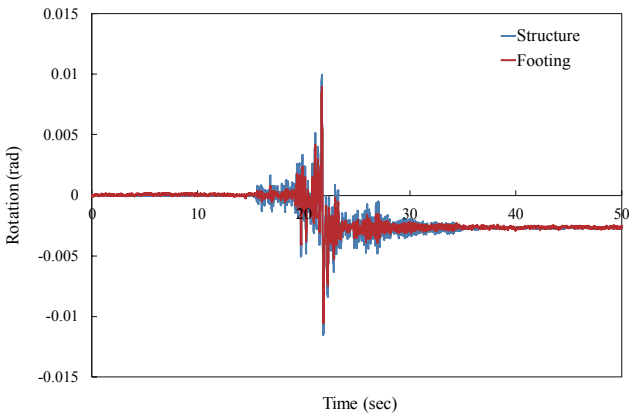

Fig. 3 Comparison of rotation histories at the top of the structure and top of the footing

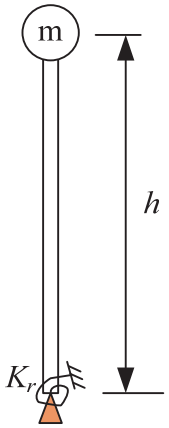

Fig. 4 Simplified single-degree-of-freedom rocking system

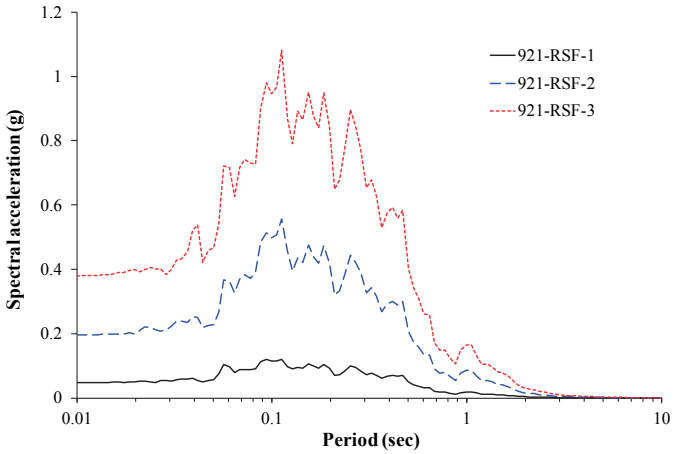

Fig. 5 Acceleration spectra of base motions

Figures 6(a) and 6(b) show the transfer functions of the structure model and soil specimen for Case WN, respectively. The fundamental frequency of the structure is 5.1 Hz, and the fundamental frequency of the soil specimen is 20 Hz. Figure 7 displays the acceleration spectra at the soil surface for Cases 921-RSF-1 to 921-RSF-3. The first significant response occurs at 0.056 sec (about 18 Hz). Compared with the white noise sweeping results, it is close to the fundamental frequency of the soil of 20 Hz. In addition, for Cases 921-RSF-2 and 921-RSF-3, another significant spectra response occurs at the period of around 0.094 sec (about 10.6 Hz), indicating that the nonlinear soil behavior is apparent in those cases with larger excitation. Next, the test data are analyzed by the system identification methods and the results are presented in the next section.

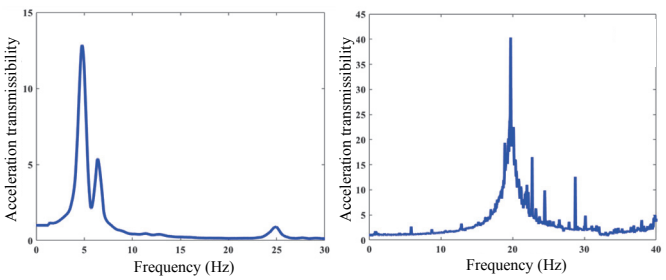

(a) Structure (b) Soil

Fig. 6 Experimental frequency response function in Case WN

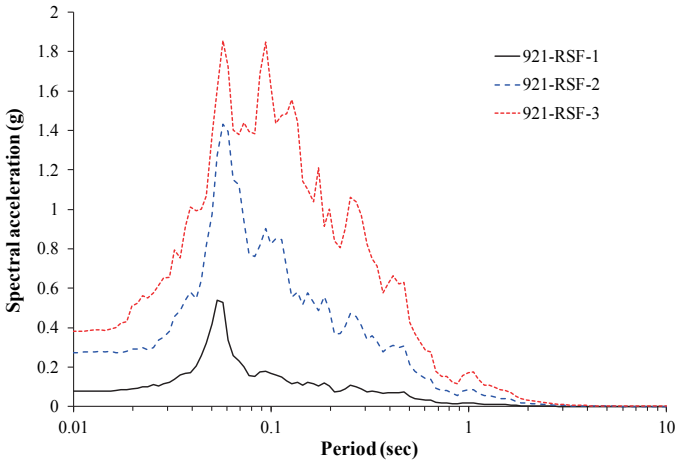

Fig. 7 Acceleration spectra of motions on the soil surface

5. SYSTEM IDENTIFICATION RESULTS AND DISCUSSION

5.1 Short-Time Transfer Function

The aforementioned segmentation scheme is adopted to perform the short-time transfer function analysis. Figures 8(a) to 8(c) show the short-time transfer functions of Cases 921-RSF-1 to 921-RSF-3. From these figures, three remarkable regions of frequency of larger amplification can be recognized. The first one is 4 to 6 Hz occurring in the initial and free vibration states. The second one is below 4 Hz during the main shaking. This shows that the fundamental frequency of the system varies during excitations. The third one is at around 24 Hz when the column-footing system is under initial and free vibration states and it is referred to as the twisting mode of the structure model as mentioned previously. Comparing these cases, it is found that the fundamental frequency decreases when the excitation intensity increases. The reduction of the fundamental frequency is due to the uplifting of the footing. Significant reduction occurs when the system is under strong rocking.

From the results shown above, the short-time transfer function can help derive the evolution of the fundamental frequency with time; however, it is not easy to read out the actual values.

5.2 Short-Time ARMA Analysis

It is straightforward for the ARMA method to identify the fundamental frequency as well as the damping ratio, and the rotational stiffness of the footing can be further deduced based on the fundamental frequency. The results of the short-time ARMA analysis for the dynamic structure characteristics under the main shaking of Cases 921-RSF-1 to 921-RSF-3 are shown in Figs. 9(a) to 9(c). The left hand-top of the figure presents the output acceleration response of the system, and the evolutions of the fundamental frequency, rotational stiffness and damping ratio are displayed at the right hand-top, left hand-bottom and right hand-bottom, respectively. Note that all the figures only display the main excitation that is of interest.

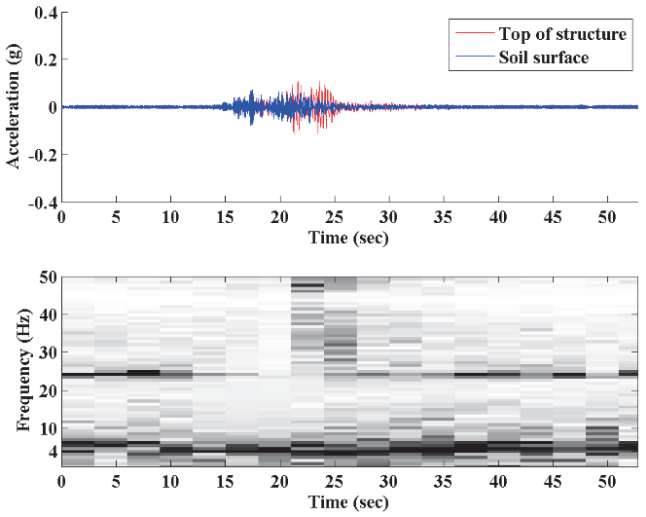

(a) Case 921-RSF-1

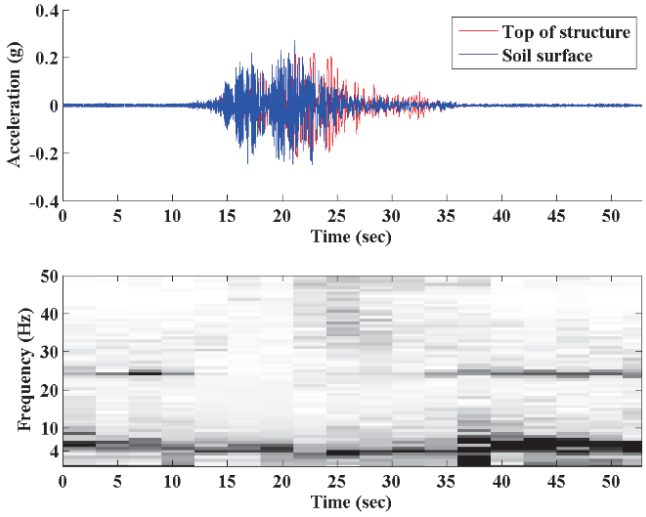

(b) Case 921-RSF-2

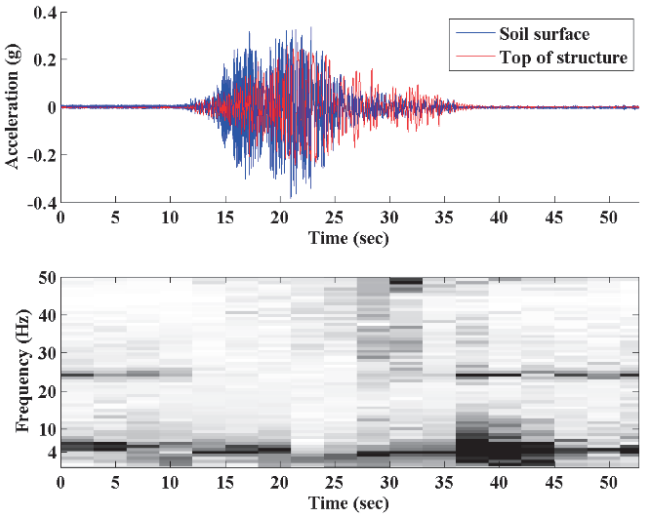

(c) Case 921-RSF-3

Fig. 8 Short-time frequency response functions for structure

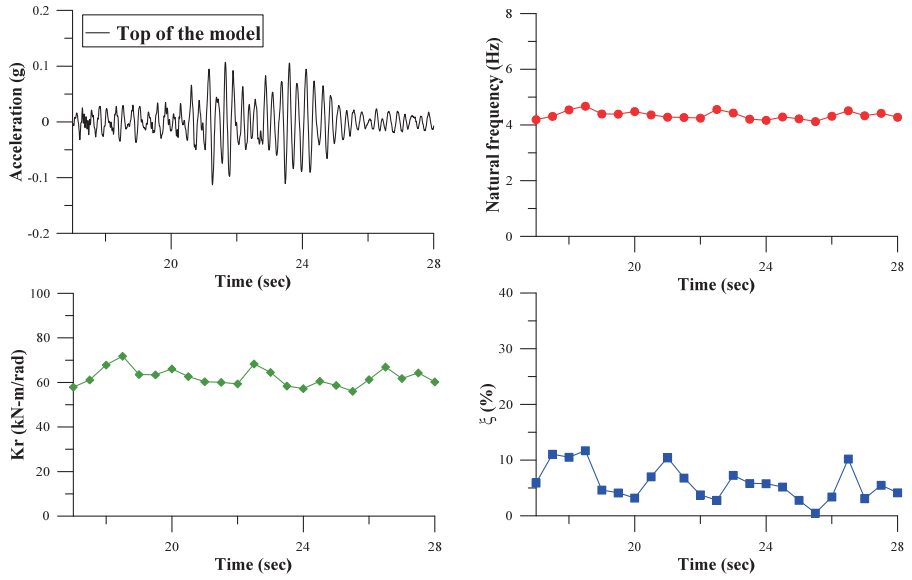

(a) Case 921-RSF-1

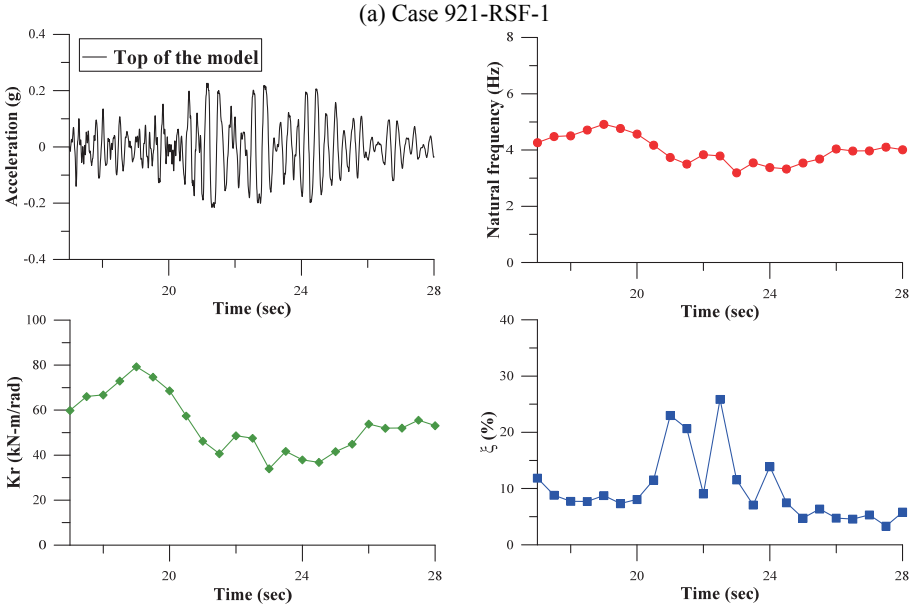

(b) Case 921-RSF-2

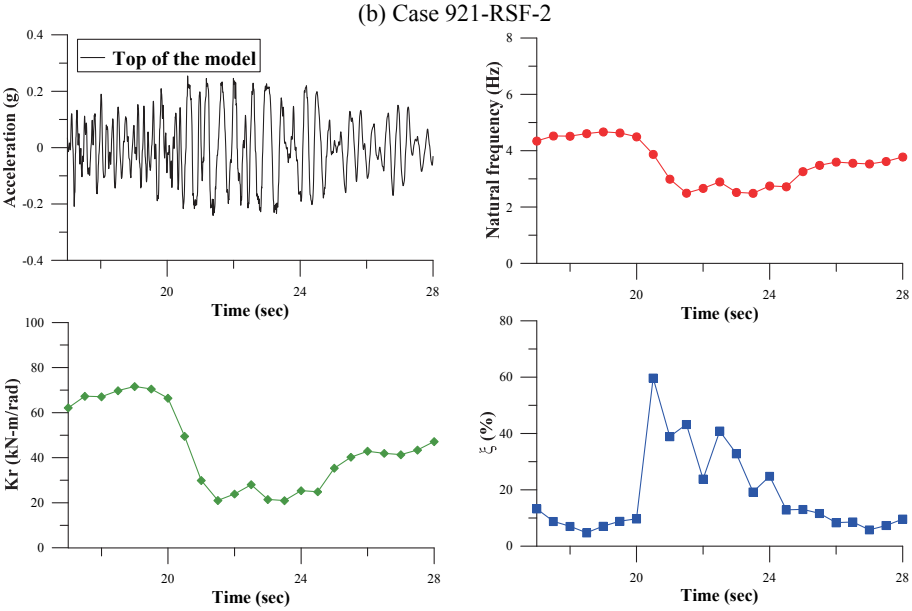

(c) Case 921-RSF-3

Fig. 9 Short-time system identification for structure

According to Gazetas *et al.* (2013), the rotational stiffness K_r of a rocking foundation system can be computed by the following equation:

$$K_r = mh^2 w_n^2 + mgh \tag{9}$$

where m and h are the mass and height of the structure, and w_n represents the natural angular frequency of the rocking structure-footing system.

In general, the identified fundamental frequency and damping ratio of the rocking foundation system would fluctuate with the intensity of excitation as shown in Figs. 10(a) to 10(c). From Fig. 10(a), it is seen that the rocking behavior is insignificant due to small excitation and the structure system exhibits a linear response most of time. The fundamental frequency of the structure model is almost the same at 4.5 Hz during the main shaking. However, as shown in Figs. 9(b) and 9(c), during strong shaking, the fundamental frequency reduces due to significant uplifting of the footing, and the rotational stiffness of footing significantly reduces accordingly.

Table 2 compares the fundamental frequencies in different states for Cases 921-RSF-1 to 921-RSF-3. Overall, the strong excitation causes larger rotations and therefore reduces the fundamental frequency of the structure. For Case 921-RSF-1, the fundamental frequency varies less; however, for Cases 921-RSF-2 and 921-RSF-3, the fundamental frequency significantly reduces during the main shaking, and, compared to the initial state, the reduction ratio of the fundamental frequency is 62% and 41% (rotational stiffness reduction ratio 38% and 17%) for Cases 921-RSF-2 and 921-RSF-3, respectively. On the other hand, although the fundamental frequency reduces during shaking, it can rise at the free vibration state when the excitation stops. However, for Case 921-RSF-3 the fundamental frequency at the free vibration state will not go back to the original state as shown in Table 2. This is because rocking induced permanent rotation causes permanent change in rotational stiffness of the footing.

For the damping effect of the structure-footing system, the range of estimated damping ratio is about between 5% and 10% for Case 921-RSF-1. For Cases 921-RSF-2 and 921-RSF-3, the damping ratio is larger because of larger excitation intensity. From the evolution of the damping ratio in Cases 921-RSF-2 and 921-RSF-3, it is seen that the damping ratio increases with increasing excitation intensity, and the maximum damping ratio occurs when the structure system reaches its peak acceleration response. The maximum damping ratio for the structure response of Cases 921-RSF-2 and 921-RSF-3 are about 26% and 60%, respectively. It is seen that rocking behavior can significantly dissipate the seismic energy when the system is under a large ground motion.

In order to evaluate the performance of the short-time ARMA method, the short-time ARMA results are further mapped on the short-time transfer function spectrum in Figs. 10(a) to 10(c). The comparisons show that the variation of identified system frequencies are consistent with those from the short-time transfer function spectra. Besides, the short-time ARMA method is straightforward to capture the variation of fundamental frequency values of the system.

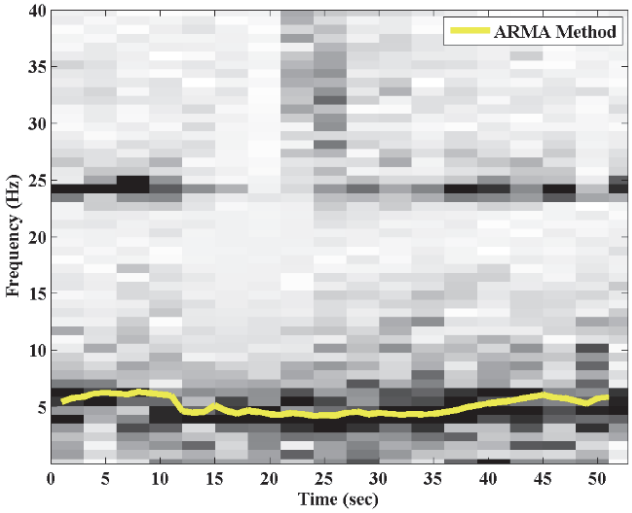

(a) Case 921-RSF-1

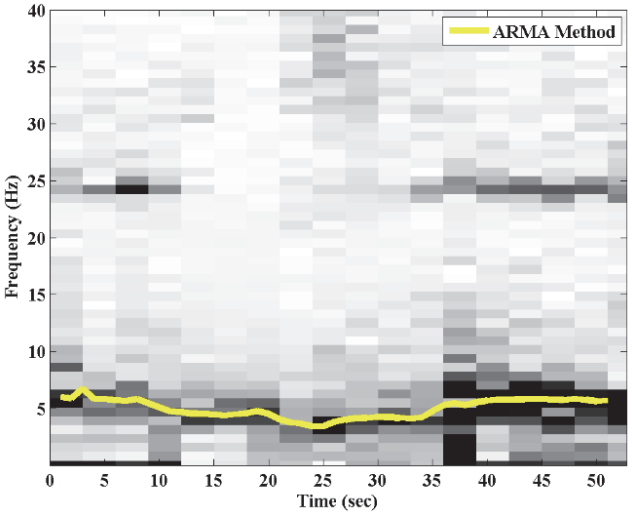

(b) Case 921-RSF-2

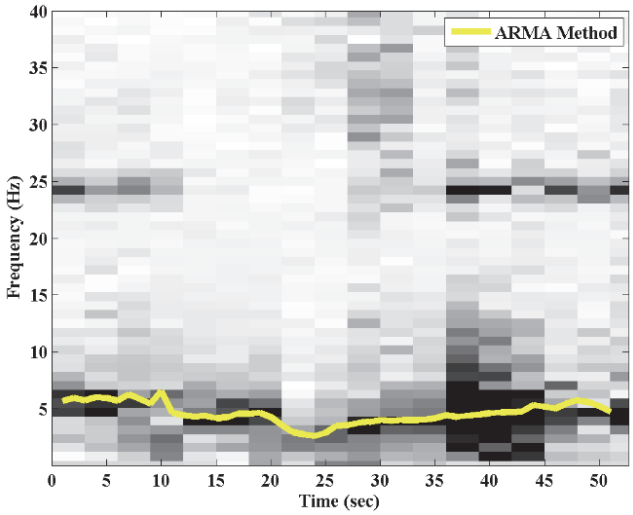

(c) Case 921-RSF-3

Fig. 10 Short-time ARMA and transfer function spectrum

Table 2 The fundamental frequencies for structure in different vibration states

Case	921-RSF-1	921-RSF-2	921-RSF-3
Frequency at initial state (Hz)	5.8	5.8	5.8
Lowest frequency during main shaking (Hz)	4.5	3.6	2.4
Frequency at free vibration state (Hz)	5.8	5.8	5.1

Table 3 Comparison of rotational stiffnesses from the short-time ARMA method and the hysteresis curve in large excitation

(Unit: kN-m/rad)

Case 921-RSF-1						
Time (sec)	17.9	21.3	21.8	22.6	23.5	26.7
Rotation (rad)	3.54E-04	1.09E-03	1.30E-03	4.23E-04	1.45E-03	2.87E-04
K_r_hys	63.9	61.4	57.3	70.3	63	59.5
K_r_SI	61.1	59.3	59.3	68.3	58.4	66.9
Case 921-RSF-2						
Time (sec)	18	21.4	22.7	23.5	24.3	26.8
Rotation (rad)	1.21E-03	6.54E-03	4.84E-03	2.29E-03	5.05E-03	1.79E-03
K_r_hys	70.6	31.3	37.1	46.8	36.4	53.8
K_r_SI	73	40.7	47.5	41.7	36.8	52
Case 921-RSF-3						
Time (sec)	18.1	21.8	23	24.2	25.5	27.2
Rotation (rad)	1.85E-03	7.97E-03	1.22E-02	7.27E-03	3.22E-03	2.57E-03
K_r_hys	69.9	23.3	17.8	24.7	38.8	46.1
K_r_SI	70.4	18.5	21	24.8	40.3	43.4

K_r_hys: the rotational stiffness calculated based on the moment-rotation loop
K_r_SI: the rotational stiffness estimated by the short-time ARMA method

Table 4 Comparison of damping ratios from the short-time ARMA method and the hysteresis curve in large excitation

Case 921-RSF-1						
Time (sec)	17.9	21.3	21.8	22.6	23.5	26.7
Rotation (rad)	3.54E-04	1.09E-03	1.30E-03	4.23E-04	1.45E-03	2.87E-04
ξ_hys (%)	18.0	18.9	11.5	21.4	8.9	14.9
ξ_SI (%)	18.6	7.0	7.0	7.9	2.8	0.5
Case 921-RSF-2						
Time (sec)	18	21.4	22.7	23.5	24.3	26.8
Rotation (rad)	1.21E-03	6.54E-03	4.84E-03	2.29E-03	5.05E-03	1.79E-03
ξ_hys (%)	13.5	23.0	17.4	14.2	14.8	8.0
ξ_SI (%)	8.8	11.5	20.7	25.9	7.1	6.4
Case 921-RSF-3						
Time (sec)	18.1	21.8	23	24.2	25.5	27.2
Rotation (rad)	1.85E-03	7.97E-03	1.22E-02	7.27E-03	3.22E-03	2.57E-03
ξ_hys (%)	11.3	20.0	22.2	21.9	11.9	9.0
ξ_SI (%)	8.8	59.7	40.9	19.2	10.7	8.6

ξ_hys: the damping ratio calculated based on the moment-rotation loop
ξ_SI: the damping ratio identified by the short-time ARMA method

5.3 Comparisons between Short-Time ARMA Analysis and Hysteresis Curves

Moment-rotation hysteresis loops characterize the response of nonlinear rotational stiffness of a footing. From the above system identification, it is shown that the system characteristics of the structure change during excitation. This section will further compare the results of the ARMA method with the experimental moment-rotation hysteresis loops among different excitation cases.

Figures 11(a) to 11(c) show the moment-rotation curves for Cases 921-RSF-1 to 921-RSF-3. In the figure, the moment is the mass times the acceleration times the height of the mass. In the small excitation case (921-RSF-1), the moment-rotation curve in each cycle is a symmetric ellipse, and the rotational stiffness is similar during the excitation. However, for Cases 921-RSF-2 and 921-RSF-3, the hysteresis loops enlarge when the dynamic response of the structure model increases, and the rotation increases as well.

The significant hysteretic behavior is due to the limitation of the moment capacity. When the model reaches the ultimate moment state, the rotation of the structure keeps increasing and therefore causes a significant hysteresis loop. Another important contribution of the hysteresis behavior is the plastic deformation of the soil underneath the foundation. Although the hysteresis curve is considered as the energy dissipation behavior for rocking behavior, it should be noticed that it is accompanied with the permanent deformation of the soil and the permanent rotation of the footing. As in Case 921-RSF-3 (Fig. 11(c)), the moving hysteresis loops are due to the significant permanent rotation of the footing.

The moment-rotation hysteresis loop can be further modeled as an equivalent-linear viscous damped system with an equivalent stiffness K_r and an equivalent damping ratio ξ. According to Chopra (1995), the equivalent rotational stiffness is the secant slope at the maximum rotation of the moment-rotation loop; based on the area of the hysteretic loop, the equivalent damping ratio ξ is obtained by equating the total dissipation energy W_D during one cycle of loading with the associated elastic strain energy W_E at the maximum rotation, which is expressed as

$$\xi=\frac{W_D}{4\pi W_E} \tag{10}$$

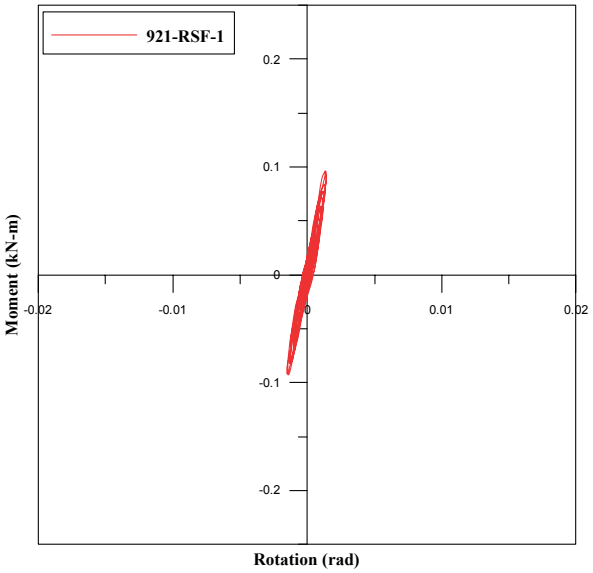

(a) Case 921-RSF-1

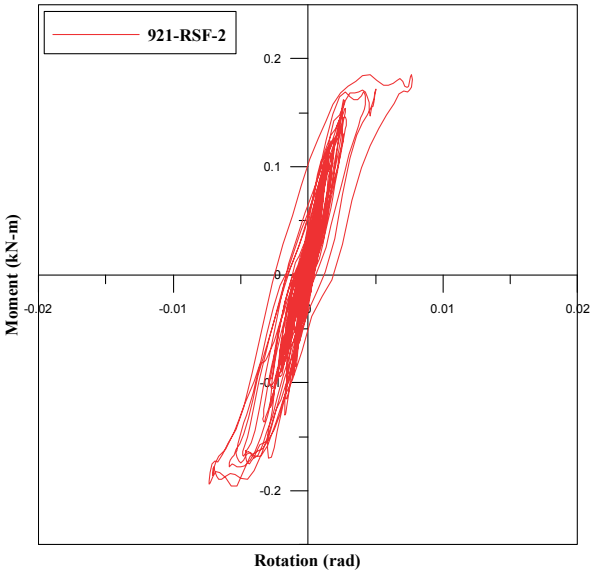

(b) Case 921-RSF-2

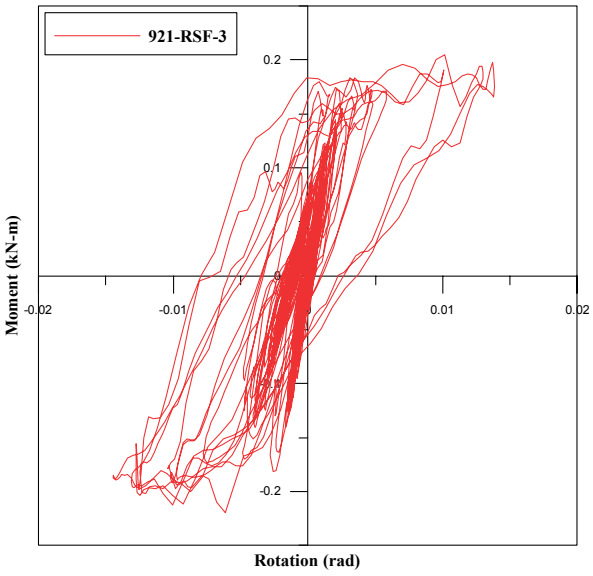

(c) Case 921-RSF-3

Fig. 11 Moment-rotation curves

Figures 12(a) to 12(c) compare estimated rotational stiffness by the short-time ARMA analysis with the moment-rotation loops of the footing for Cases 921-RSF-1 to 921-RSF-3. The selected time sections are within the main shaking duration or the time interval in which significant rocking occurs. In these figures, the red lines with red dots represent the moment-rotation curve at certain time sections, and the blue lines represent the identified rotational stiffness by system identification. The time section of 0.5 sec for system identification is adopted in building the moment-rotation curve. In Cases 921-RSF-1 to 921-RSF-3, the identified rotational stiffness is consistent with the equivalent rotational stiffness of the hysteresis loop. It is also shown that the short-time ARMA model can capture the changes in the system stiffness. Based on the above comparisons, Table 3 summarizes the identified rotational stiffness and the back-calculated stiffness from the hysteresis curves. For a hysteresis loop, the equivalent rotational stiffness is the secant slope at the maximum rotation of the moment-rotation loop.

Table 4 summarizes the identified damping ratio and the back-calculated damping ratio from the hysteresis curves. Both the results of system identification and the hysteretic loops showed that rocking behavior can dissipate the seismic energy; however, there are some differences between them, which is because the rotational spring is assumed to be linear in the ARMA model, but the hysteresis loops are actually nonlinear.

Based on Table 3, Fig. 13(a) plots the relationship of identified rotational stiffness vs. rotation. Three cases show consistent trends: the rotational stiffness is about constant at the small rotation level (< 0.002 rad) and for large rotations, it significantly decreases with increasing rotation. Deng *et al.* (2014) proposed an empirical equation for the initial rotational stiffness of a footing as

$$K_{r,\text{ini}} \approx 300 M_{c\text{-foot}} \tag{11}$$

where $M_{c\text{-foot}}$ is the moment capacity of the footing. In this case, $M_{c\text{-foot}}$ is 0.214 kN-m and $K_{r,\text{ini}}$ = 64.2 kN-m/rad. Compared to the rotational stiffness identified, it is interesting to note in Fig. 15(a) that the $K_{r,\text{ini}}$ is close to the rotational stiffness at small rotations (θ < 0.002 rad). Besides, for the degradation of rotational stiffness, in terms of a theoretical maximum stiffness $K_{r,\max}$ proposed by Gazatas (1991), Gajan *et al.* (2005) proposed a mean rotational stiffness reduction trend for different levels of rotation based on centrifuge tests, as follows,

$$\frac{K_r}{K_{r,\max}} = 3.0\times10^{-3}(\theta^{-0.6}) \tag{12}$$

For this study, according to Gajan *et al.* (2005), $K_{r,\max}$ of 669 kN-m/rad is estimated. The trend of rotational stiffness at different levels of rotation is built as shown in Fig. 13(a). It is seen that Eq. (12) appears to be the upper bound of the rotational stiffness identified; however, at low rotations (< 0.003 rad), the rotational stiffness seems to be much overestimated. The empirical $K_{r,\text{ini}}$ is much smaller than the theoretical $K_{r,\max}$. This is because the theoretical $K_{r,\max}$ ignores soil plasticity and footing uplift. Besides, a curved soil surface was possibly formed below the foundation base during repetitive rocking, causing a smaller contact area between the soil and footing and leading to a lower rotational stiffness (Gajan *et al.* 2005; Paolucci *et al.* 2008). Regarding $K_{r,\text{ini}}$ as the rotational stiffness prior to 50% of moment capacity (Deng

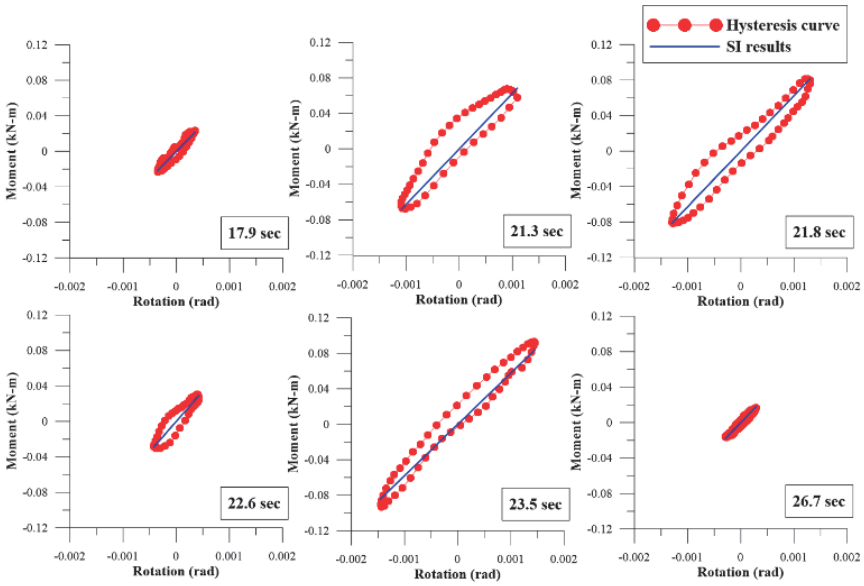

(a) Case 921-RSF-1

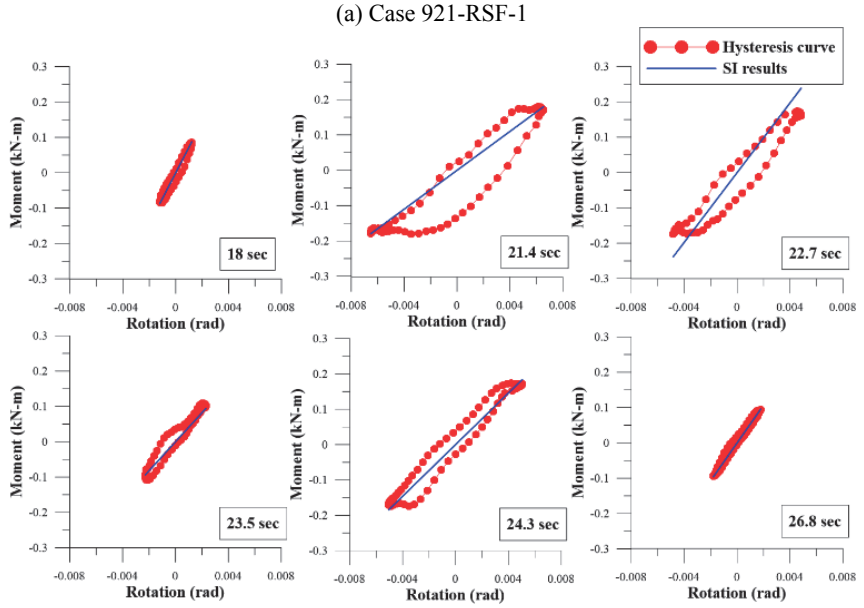

(b) Case 921-RSF-2

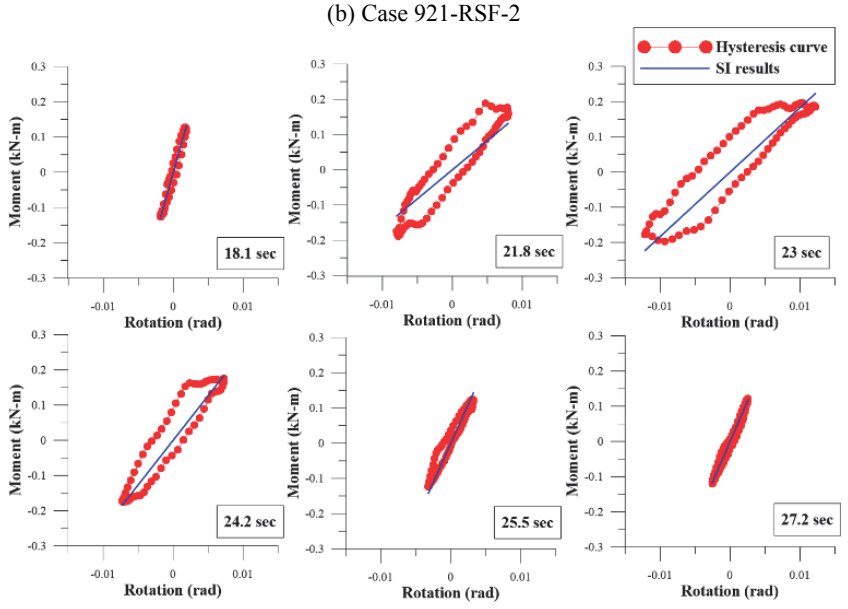

(c) Case 921-RSF-3

Fig. 12 Moment-rotation curves versus identified rotational stiffnesses

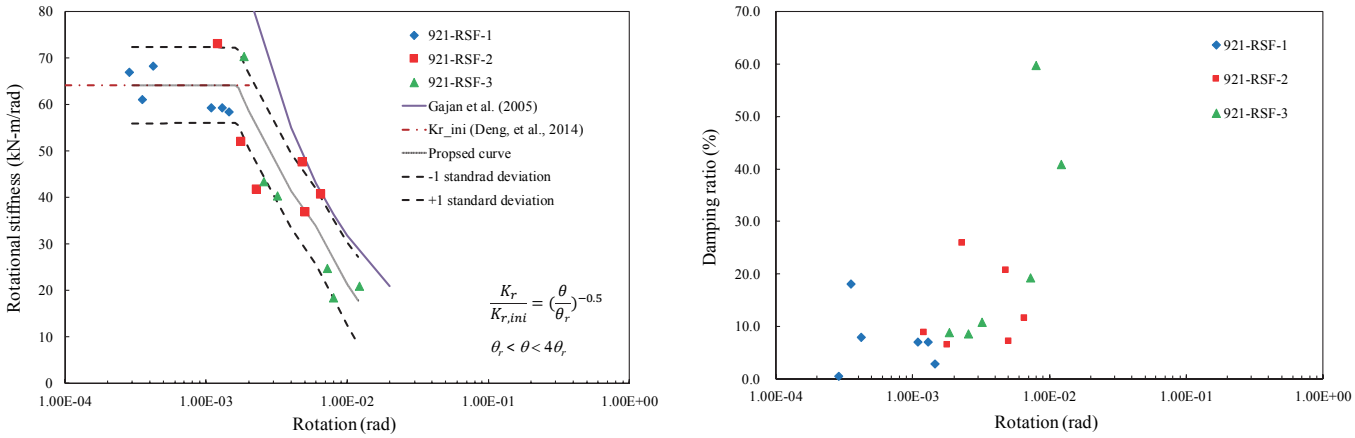

(a) Rotational stiffness (b) Damping ratio

Fig. 13 Relationships of identified rotational stiffness and identified damping ratio *vs.* rotation

et al. 2014), based on the data points, a mean relationship for the reduction trend of rotational stiffness with respect to $K_{r,\text{ini}}$ is built as follows and shown in 13(a),

$$\frac{K_r}{K_{r,\text{ini}}} = \left(\frac{\theta}{\theta_r}\right)^{-0.5} \tag{13}$$

where θ_r is the reference rotation which is 0.00167 rad, defined as $M_{c\text{-foot}}/(2K_{r,\text{ini}})$.

Equation (13) applies to $\theta_r \le \theta \le 4\theta_r$. When $\theta < \theta_r$, $K_r = K_{r,\text{ini}}$. θ is limited to be below $4\theta_r$ to avoid a moment value ($K_r\theta$) that is larger than $M_{c\text{-foot}}$. In addition, Fig. 13(a) also displays upper and lower bound curves for ±1 standard deviation, respectively.

Based on Table 4, Fig. 13(b) plots the relationship of identified damping ratio vs. rotation. The damping ratio appears to increase with the amplitude of rotation. Along with the trend of rotational stiffness vs. rotation, at small rotations (< 0.002 rad), the damping ratio is low (most data are about 6% to 9%); afterward the damping ratio significantly increases with increasing rotation. Overall, the damping ratio is low for the case with low intensity of shaking while the damping ratio is large for the case with strong intensity of shaking due to large rotations generated.

6. CONCLUSIONS

In this study, two methods of system identification have been applied to investigate the changes in the dynamic system characteristics of a column-footing-soil model in the shaking table testing under different excitation conditions. The results of system identification were further compared with the experimental hysteretic moment-rotation loops to interpret the meaning of the identified system parameters. The following conclusions can be drawn.

(1) With the aid of the segmentation scheme, the short-time transfer function and ARMA method can effectively capture the evolution of the dynamic system frequency of the column-footing model. Compared to the transfer function method, the ARMA method can also identify the damping ratio of the system and it is more straightforward for the ARMA method to determine the values of the system frequency.

(2) During the process of shaking, the fundamental frequency of the model is not constant. The fundamental frequency decreases as the shaking intensity increases, but it may increase as the shaking intensity decreases. The reduction of fundamental frequency implies the degradation of rotational stiffness of the footing due to the uplift of the footing. Especially for the largest excitation case in this study, the rotational stiffness of the footing is reduced to only 17% and does not go back to the original state after excitation due to the permanent rotation.

(3) The change in the identified damping ratio follows the variation trend of the fundamental frequency. The damping ratio increases as the fundamental frequency decreases, and the maximum damping ratio occurs when the fundamental frequency is about to reach its lowest value.

(4) The identified dynamic properties are compatible with those determined from the hysteretic moment-rotation curves. The ultimate moment capacity of the footing limited the structure acceleration, which causes a low rotational stiffness and a high damping ratio identified at large excitation intensity.

ACKNOWLEDGEMENTS

The authors would like to thank the Ministry of Science and Technology of Taiwan (Grant No. MOST 104-2221-E-002-218) for financial support.

REFERENCES

AASHTO (2009). *Guide Specifications for LRFD Seismic Bridge Design*, American Association of State Highway and Transportation Officials, Washington, D.C., U.S.A.

Anastasopoulos, I. and Kontoroupi, T. (2014). "Simplified approximate method for analysis of rocking systems accounting for soil inelasticity and foundation uplifting." *Soil Dynamics and Earthquake Engineering,* **56**, 28-43. https://doi.org/10.1016/j.soildyn.2013.10.001

Chiou, J.S., Chen, C.H., and Huang, Y.W. (2018). "Pushover and shaking table tests on a rocking-governed column-footing model on dry dense sand." *Journal of the Chinese Institute of Engineers*, **41**(3), 247-258. https://doi.org/10.1080/02533839.2018.1454858

Chopra, A.K. (1995). *Dynamics of Structures*. Prentice-Hall, Upper Saddle River, NJ., U.S.A.

Deng, L., Kutter, B.L., and Kunnath, S.K. (2014). "Seismic design of rocking shallow foundations: displacement-based methodology." *Journal of Bridge Engineering,* ASCE, **19**(11), 04014043. https://doi.org/10.1061/(ASCE)BE.1943-5592.0000616

Elgamal, A.W., Zeghal, M., Parra, E., Gunturi, R., Tang, H.T., and Stepp, J.C. (1996). "Identification and modeling of earthquake ground response — I. Site amplification." *Soil Dynamics and Earthquake Engineering,* **15**(8), 499-522. https://doi.org/10.1016/S0267-7261(96)00021-8

Gajan, S. and Kutter, B.L. (2008). "Capacity, settlement, and energy dissipation of shallow footings subjected to rocking." *Journal of Geotechnical and Geoenvironmental Engineering,* ASCE, **134**(8), 1129-1141. https://doi.org/10.1061/(ASCE)1090-0241(2008)134:8(1129)

Gajan, S. and Kutter, B.L. (2009). "Contact interface model for shallow foundations subjected to combined cyclic loading." *Journal of Geotechnical and Geoenvironmental Engineering,* ASCE, **135**(3), 407-419. https://doi.org/10.1061/(ASCE)1090-0241(2009)135:3(407)

Gajan, S., Kutter, B.L., Phalen, J.D., Hutchinson, T.C., and Martin, G.R. (2005). "Centrifuge modeling of load-deformation behavior of rocking shallow foundations." *Soil Dynamics and Earthquake Engineering,* **25**(7), 773-783. https://doi.org/10.1016/j.soildyn.2004.11.019

Gazetas, G. (1991). "Foundation vibrations." Fang, H-Y,, Ed., *Foundation Engineering Handbook.* Chapter 15, van Nostrand Reinhold; New York, U.S.A.

Gazetas, G., Anastasopoulos, I., Adamidis, O., and Kontoroupi, T. (2013). "Nonlinear rocking stiffness of foundations." *Soil Dynamics and Earthquake Engineering,* **47**, 83-91. https://doi.org/10.1016/j.soildyn.2012.12.011

Glaser, S.D. (1995). "System identification and its application to estimating soil properties." *Journal of Geotechnical Engineering,* ASCE, **121**(7), 553-560. https://doi.org/10.1061/(ASCE)0733-9410(1995)121:7(553)

Glaser, S.D. and Baise, L.G. (2000). "System identification estimation of soil properties at the Lotung site." *Soil Dynamics and Earthquake Engineering,* **19**(7), 521-531. https://doi.org/10.1016/S0267-7261(00)00026-9

Mikami, A., Sawada, T., and Ekawa, T. (2003). "Identification of non-linear and non-stationary soil properties during the 1995 Hyogoken-nanbu earthquake." *Soil Dynamics and Earthquake Engineering,* **23**(4), 279-286. https://doi.org/10.1016/S0267-7261(03)00002-2

Paolucci, R., Shirato, M., and Yilmaz, M.T. (2008). "Seismic behaviour of shallow foundations: Shaking table experiments vs numerical modelling." *Earthquake Engineering and Structural Dynamics,* **37**(4), 577-595. https://doi.org/10.1002/eqe.773

Polhemus, N.W. and Cakmak, A.S. (1981). "Simulation of earthquake ground motions using autoregressive moving average (ARMA) models." *Earthquake Engineering and Structural Dynamics,* **9**(4), 343-354. https://doi.org/10.1002/eqe.4290090404

Safak, E. (1989). "Optimal-adaptive filters for modelling spectral shape, site amplification, and source scaling." *Soil Dynamics and Earthquake Engineering,* **8**(2), 75-95. https://doi.org/10.1016/S0267-7261(89)80015-6

Shirato, M., Kouno, T., Asai, R., Nakatani, S., Fukui, J., and Paolucci, R. (2008). "Large-scale experiments on nonlinear behavior of shallow foundations subjected to strong earthquakes." *Soils and Foundations,* **48**(5), 673-692. https://doi.org/10.3208/sandf.48.673

Zeghal, M., Elgamal, A.W., Tang, H.T., and Stepp, J.C. (1995). "Lotung downhole array. II: Evaluation of soil nonlinear properties." *Journal of Geotechnical Engineering,* ASCE, **121**(4), 363-378. https://doi.org/10.1061/(ASCE)0733-9410(1995)121:4(363)